71st International Astronautical Congress, The CyberSpace Edition, 12-14 October 2020.

IAC–20–A6,2,12,x58045

AI for Autonomous CAM Execution

Luis Sánchez Fernández-Mellado
University of Strathclyde, Glasgow, UK, luis.sanchez-fdez-mellado@strath.ac.uk

Massimiliano Vasile
University of Strathclyde, Glasgow, UK, massimiliano.vasile@strath.ac.uk

Abstract

This paper combines a previously developed Intelligent Classification Systems (ICS) for collision risk prediction with a simple Collision Avoidance Manoeuvre (CAM) allocation procedure. The Intelligent Classification System is based on a combination of Evidence Theory for collision risk assessment and a Machine Learning model that classifies conjunction events given the encounter geometry, the uncertainty in the probability of collision and the time at which the conjunction event occurs.
We introduce a quick method to compute a Collision Avoidance Manoeuvre when the Intelligent Classification System suggests that a CAM is needed. The method presented in this paper accounts for epistemic uncertainty in the collision prediction. The inclusion of the epistemic uncertainty requires solving a min-max problem to find the optimal impulse for the worst-case scenario. Finally, the paper introduces the basis for a future ML-based system able to predict the optimal CAM under epistemic uncertainty.
keywords: Space Traffic Management, Artificial Intelligence, Machine Learning, Collision Avoidance Manoeuvre, min-max optimisation, Epistemic Uncertainty

Acronyms

AI Artificial Intelligence.

ANN Artificial Neural Network.

bpa Basic Probabilistic Assumption.

CAM Collision Avoidance Manoeuvre.

DSt Dempster-Shafer theory of Evidence.

FE Focal Element.

HBR Hard Body Radius.

ICS Intelligent Classification System.

ML Machine Learning.

$\mathbf{P}_C$ Probability of Collision.

RF Random Forest.

STM Space Traffic Management.

TCA Time of Closest Approach.

1. INTRODUCTION

The increase on the launches rate during the last years and the emergence of new Mega-Constellation with thousands of satellites already on deployment along with the growing number of space debris objects, makes the Space Safety no longer guaranteed.[1,2] To ensure the safe operation of satellites in orbit, Space Traffic Management (STM) system requires new techniques and modifications affecting different areas[3]: close encounter detection, automatic risky event classification, or autonomous Collision Avoidance Manoeuvre (CAM) design.

Among those new techniques, Artificial Intelligence (AI) and Machine Learning (ML) appear as good candidates to improve the STM system. AI and ML are able to cope with the great amount of information expected to be available the next years and even learn from the new data collected, allow the automation of the system required to handle the expected increase on encounter alerts, and perform faster than dynamic-based methods, which helps on automation.

Some works have been already developed on the application of ML to improve and support STM operations: autonomous Intelligent Classification System of risky events,[4] automatic Artificial Neural Network (ANN)-based close encounter detection,[5] orbit error

propagation using ML,[6] or automatic application of Collision Avoidance Manoeuvre.[7]

In this paper, the Intelligent Classification System (ICS) presented in Sanchez and Vasile[4] is the starting point to introduce a step further in the development of an Intelligent Agent capable to autonomously predict collisions, determine whether a CAM is required, execute the manoeuvre, and detect again potential encounters along the new orbit.

The Intelligent Classification System uses an evidences-based event classification criterion accounting for the epistemic uncertainty affecting the space objects' position. The system makes use of Random Forest (RF)[8] to propose the best action to be implemented when a close encounter is detected.

When the ICS classifies a conjunction event like a collision, a possible recommendation is to perform a Collision Avoidance Manoeuvre. In this paper, we present a modification of a simple linear model to calculate an optimal CAM. Different authors have proposed linear models for computing the optimal direction of the impulse manoeuvre.[9–11] In this work, a variation of the approach proposed by Vasile and Colombo[9] has been implemented.

The novel approach followed on this paper is the inclusion of epistemic uncertainty in the calculation of the CAM. The epistemic uncertainty is quantified with Dempster-Shafer Theory of Evidence (DSt),[12] which requires solving a min-max optimisation problem[13,14] in order to find the optimum CAM for the worst-case scenario.

The rest of the paper is structured as follows: in Section 2, the evidence-based risk assessment accounting for epistemic uncertainty approach is presented. Section 3 includes the Intelligent Classification System performances based on the evidence-based classification criterion. Section 4 explains how the Linear Model for CAM can be used for executing a manoeuvre when the Intelligent Classification System classifies an event as high risk and introduces the path for a future ML-based CAM execution system. Finally, Section 5 concludes the paper and presents future works.

2. EVIDENCE-BASED RISK ASSESSMENT

In this section, the quantification of epistemic uncertainty for collision risk assessment and the evaluation of the risk based on the degree of belief on the value of Probability of Collision is presented.

2.1 *Dilution of Probability of Collision*

The Probability of Collision, P_C, is a common metric used on Collision Risk Assessment. It is usually computed under the assumption of short-term encounter[15]: i) the relative motion between objects is assumed to be rectilinear; ii) the uncertainty distributions of the positions of the two bodies are Gaussian and uncorrelated; iii) the velocity vectors are not uncertain; iv) the objects are modelled as hard spheres. This assumption allows reducing the computation of P_C to the double integral of the 2D Normal Distribution over the area delimited by the Hard Body Radius (HBR) of the combined two objects[15]:

$$P_C = \frac{1}{2\pi\sqrt{||\mathbf{\Sigma}||}} \int\limits_{\mathcal{B}((0,0),R)} e^{-\frac{1}{2}\left(\mathbf{r_e}\mathbf{\Sigma}^{-1}\mathbf{r_e}\right)} d\xi d\zeta \quad [1]$$

with $\mathbf{r_e} = [\mu_\xi \;\; 0 \;\; \mu_\zeta]$ the miss distance of the centre of the ellipsoid in the B plane and $\mathbf{\Sigma}$ the covariance matrix. It simplifies into Equation (2) when the ellipse is aligned with the B plane reference frame:

$$P_C = \frac{1}{2\pi\sigma_\xi\sigma_\zeta} \int\limits_{\mathcal{B}((0,0),R)} e^{-\frac{1}{2}\left(\frac{(\xi-\mu_\xi)^2}{\sigma_\xi^2}+\frac{(\zeta-\mu_\zeta)^2}{\sigma_\zeta^2}\right)} d\xi d\zeta \quad [2]$$

Eq. (2) leads to the known paradoxical phenomenon of dilution of probability[16]. Thus, given an encounter, when the uncertainty increases, quantified exclusively as an increase on the covariance, at the beginning the P_C also rises until reaching a maximum, after which it starts decreasing. This seems to suggest that the reduction in the amount of information on the satellite's position reduces the P_C. This effect is not just counterintuitive, but also leads to false confidence for operators on the satellites' safety[17].

The reason behind this phenomenon can be seen in Figure 1: when uncertainty is only modelled as purely aleatory (an irreducible random process), the area on the bounded region under the Normal Distribution decreases when the curve flattens due to the increase on the standard deviation, describing and actual reduction on P_C[17]. However, when uncertainty is epistemic, the reasoning should lead to the conclusion that a higher ignorance corresponds to a higher risk of a collision.

In the following, we maintain the calculation of the P_C with Eq. (2) but we propose to model the epistemic uncertainty in the observations using Dempster-Shafer Theory of Evidence (DSt).[12] In particular, we consider the case in which the values of $[\mu_\xi, \mu_\zeta]$ and $[\sigma_\xi, \sigma_\zeta]$ are partially known and we can

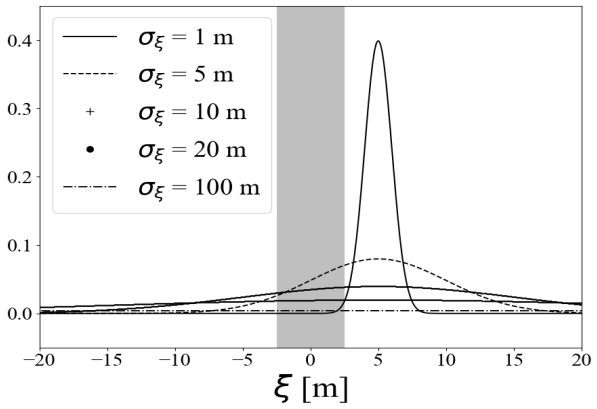

Fig. 1: Flatten of the Normal Distribution curve when standard deviation increases. The grey area (HBR) below the curves makes larger for low values of σ_ξ ($\sigma_\xi < 5m$) but decrease for higher values ($\sigma_\xi > 5m$). $HBR = 5m$ and $\mu_\xi = 5m$.

assign a degree of belief (or confidence) to the set to which they belong. This situation can derive, for example, from the fusion of different conflicting observations or from a lack of knowledge on the quality of the sensors.

2.2 *Evidence Theory*

In this section, we provide a brief description of the main features of DSt that will be used in the remainder of the paper. In DSt one can associate a degree of belief in the realisation of an event without an exact knowledge of an associated probability distribution.

Given an event space, the set Θ of all the mutually exclusive and collectively exhaustive elementary events (or hypotheses) $\Theta = \{\theta_1, \theta_2, ..., \theta_{|\Theta|}\}$ is considered. The collection of all non empty subsets of Θ, including the Empty Space and Θ itself, is the Power Set $2^\Theta = (\Theta, \cup)$. One can now assign a probability mass, called basic probability assignment (*bpa*), to the elements of 2^Θ. Each element of 2^Θ with a non-zero *bpa* is called a *Focal Element* (FE) and is represented with the symbol γ in the following. The *bpa* functions have the following properties:

$$bpa(\emptyset) = 0 \quad [3]$$

$$\forall \gamma_i \in \Gamma, 0 \leq bpa(\gamma_i) \leq 1 \quad [4]$$

$$\sum bpa(\gamma_i) = 1, \forall \gamma_i \in \Gamma \quad [5]$$

In this work, the pair $\langle \Gamma, bpa_\Gamma \rangle$ - where $\Gamma \ni \gamma$ and $bpa_\Gamma \ni bpa_\gamma$ - is called the *Body of Evidence* and the power set $U = 2^\Theta$ the *Uncertainty Space*. Considering now the set:

$$\Omega = \{\mathbf{u} \in U | f(\mathbf{u}) \in \Phi\} \quad [6]$$

where f is a quantity of interest, $\mathbf{u}$ a vector of uncertain parameters and Φ is a desirable target set for f. Given Ω, we define the two quantities, Belief (Bel) and Plausibility (Pl):

$$Bel(\Omega) = \sum_{\gamma_i \subset \Omega, \gamma_i \in U} bpa(\gamma_i), \quad [7]$$

$$Pl(\Omega) = \sum_{\gamma_i \cap \Omega \neq \emptyset, \gamma_i \in U} bpa(\gamma_i), \quad [8]$$

which give, respectively, the lower and upper limit on our confidence on Ω given the available evidence supporting statement, Eq. (6). Belief and Plausibility have the following properties:

$$Bel(\Omega) + Pl(\neg\Omega) = 1 \quad [9]$$

$$Bel(\Omega) + Bel(\neg\Omega) \leq 1 \quad [10]$$

$$Pl(\Omega) + Pl(\neg\Omega) \geq 1 \quad [11]$$

$$Pl(\Omega) \geq Bel(\Omega) \quad [12]$$

The difference between Belief and Plausibility, $\Delta(\Omega) = Pl(\Omega) - Bel(\Omega)$, associated with Ω, is called *Degree of Confidence* and can be used to determine the degree of epistemic uncertainty associated with an event given the available evidence. This concept will be exploited in this paper to classify conjunction events.

2.3 *Evidence Theory for Collision Risk Assessment*

The idea is that when $[\mu_\xi, \mu_\zeta]$ and $[\sigma_\xi, \sigma_\zeta]$ are affected by epistemic uncertainty, their values are not precisely defined and we can only say that they belong to a given set with a given degree of belief. A higher uncertainty translates into a larger set or in more, possibly disjoints, focal elements.

The evidence on the values of $[\mu_\xi, \mu_\zeta]$ and $[\sigma_\xi, \sigma_\zeta]$ comes from our degree of knowledge or ignorance on the source of the observations and the associated *bpa* assignment can come from a subjective opinion on the reliability of the source or from quantitative analysis.

Given the belief the sources assigned to the uncertain variables and their *bpa*, it is possible to compute the P_C associated with the pieces of evidence and its corresponding Belief and Plausibility.

Noting that P_C now belongs to a set since $[\mu_\xi, \mu_\zeta]$ and $[\sigma_\xi, \sigma_\zeta]$ also do, calling $f = P_C$ and the desired set of value for P_C, $\Phi = \{P_C | P_C < P_{C0}\}$, and defining the join uncertain space U so that

$\mathbf{u} = [\mu_\xi, \mu_\zeta, \sigma_\xi, \sigma_\zeta]^T$, it is possible to compute the *Bel* and *Pl* on the correctness of the value of P_C using Eqs. (7) and (8), taking $\Omega = \{\mathbf{u} \in U | P_C(\mathbf{u}) \in \Phi\}$.

In Figs. 2 and 3, an illustrative example of this approach is presented. Only for this example, the uncertain variables have been reduced to two: μ_ξ and σ_ξ. Two sources of information are supposed to provide uncertain information on the encounter geometry parameters, which translates into two different families of uncertain ellipses. A data-fuse of the sources is carried out for creating the joint uncertain space. Table 1 includes the information provided by the sources. The HBR has been taken as $R_{HBR} = 5m$ and centre in $(0, 0)$. Two scenarios are presented on the figures: a) both sources are equally reliable, thus, the *bpa* = 0.5 for both, b) one source is more reliable, with a *bpa* assignment of 0.9 and 0.1, respectively.

Table 1: Encounter parameters provided by Source 1 and Source 2.

Variable	Source 1	Source 2
μ_ξ [m]	[4,7]	[15,20]
μ_ζ [m]	5	6
σ_ξ [m]	[1,2.5]	[2,6]
σ_ζ [m]	3	3

In Fig. 2, the uncertain families distribution are presented. The green ellipses are associated with Source 1, the blue ellipses with Source 2. It can be seen that although partially overlapping, the two sources do not give coherent information. The red ellipse represents the single joint distribution used for computing the $\hat{P_C}$ if only using Eq. (2).

Given the conflict between the two sources, it is clear that there is a degree of epistemic uncertainty that cannot be neglected in the computation of P_C. Thus we can now try to use DSt to capture this epistemic uncertainty and derive a quantification of the uncertainty in the value of P_C.

Fig. 3 includes the Plausibility and Belief distribution for the examples presented in Fig. 2. The gap between both curves represents the degree of conflict between them. It can be seen that it is smaller when one source if assigned a larger *bpa*. At the same time, it can be seen that the $\hat{P_C}$ value obtained with Eq. (2) falls in a region with a low degree of confidence (big gap between *Pl* and *Bel*), which indicates that this value cannot be reliable due to the high degree of uncertainty by which it is affected.

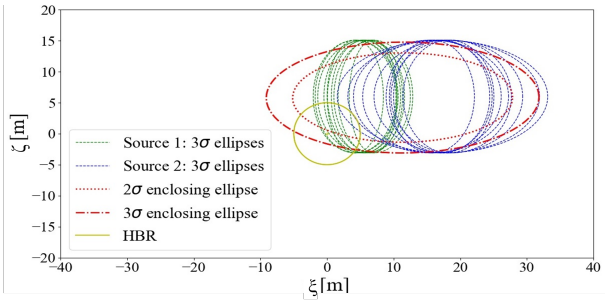

(a)

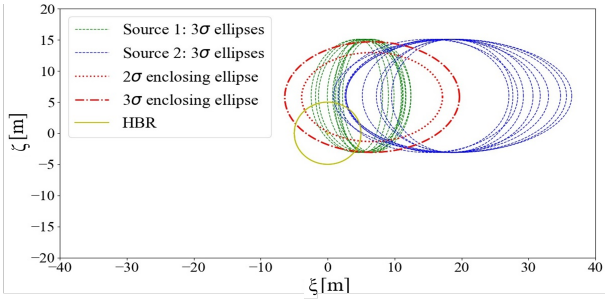

(b)

Fig. 2: Conjunction geometry on the impact plane, centred on the secondary body: (a) sources Equally reliable, (b) sources not equally reliable. Source 1 (dotted green) and Source 2 (dotted blue) represent the families of Normal Distributions provided by intervals. The ellipse enclosing both families of distributions is represented in red: 2σ (dash red) and 3σ (dash-dotted red) ellipses. The HBR is represented by the yellow solid line.

3. INTELLIGENT CLASSIFICATION SYSTEM

In this section, an Intelligent Classification System based on an evidence-based criterion classification is presented.

3.1 *Evidence-based classification criterion*

There are currently classification methods based solely on the value of P_C to trigger actions. These methods activate or not those actions when the Probability of Collision is found to be higher or lower than a given threshold. However, no information is given on the correctness of P_C. Thus the operator might react to false positives or do nothing in the case of false negatives. Furthermore, unknown cases, which require further observations, are identified only by the thresholds and not by an actual quantification of the degree of ignorance on the probability of a collision. This kind of methods can be found in the Conjunc-

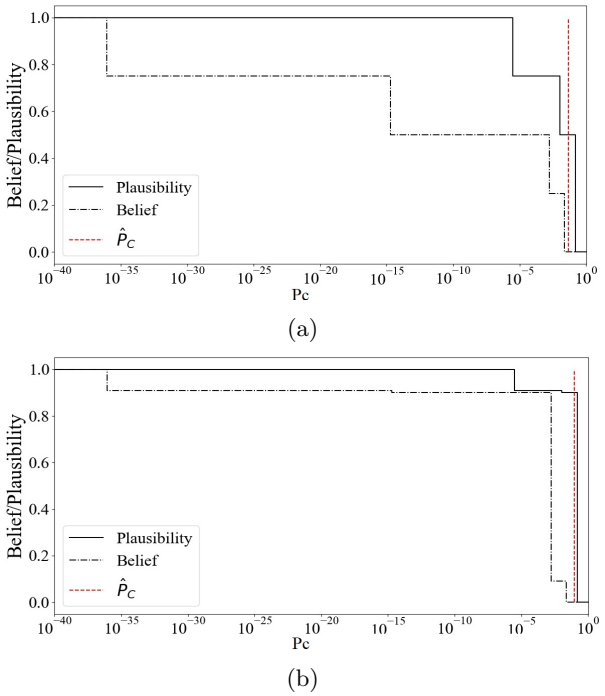

Fig. 3: Belief (dash line) and Plausibility (solid line) curves for the geometry in Fig. 2 and $\hat{P}_C$ for the combined ellipse (red vertical dash line): (a) equally reliable sources; (b) Source 1 more reliable than Source 2.

tion Assessment Risk Analysis team of NASA[18] and the Space Debris Office of ESA.[19]

In an evidence-based classification criterion three additional pieces of information may be available to the operator: the value of Bel, the value of Pl and the gap between the two at the threshold. A large gap between Pl and Bel implies that there is a lack of information on the calculation of P_C. If both Pl and Bel are low then there is little evidence that the value of P_C is to be trusted. Finally, if Bel is low one should be wary that the evidence fully supporting the value of the P_C is low.

Table 2 includes the evidence-based classification criterion used in this paper. It takes into account the time to the encounter (or time to the Time of Closest Approach, TCA), the value P_{C_b} at which the belief jumps above a certain threshold, Bel_0, and the degree of confidence, $\Delta(P_{C_0})$, or gap between Pl and Bel, at the Probability of Collision threshold, P_{C_0}.

The class refers on the last column of Table 2 encodes a suggested action to be considered by the operators: Class 1 means a CAM should be executed to avoid an imminent risky event or an event that, even

Table 2: Evidence-based classification criterion.

Time to TCA	**P_C for $Bel = Bel_0$**	**Degree of confidence at P_{C_0}**	**Class**
$t_{TCA} < T_1$	$P_{C_b} \geq P_{C_0}$	-	1
	$P_{C_b} < P_{C_0}$	$Pl - Bel \leq \Delta$	5
		$Pl - Bel > \Delta$	1
$T_1 \leq t_{TCA}$ $t_{TCA} < T_2$	$P_{C_b} \geq P_{C_0}$	-	2
	$P_{C_b} < P_{C_0}$	$Pl - Bel \leq \Delta$	5
		$Pl - Bel > \Delta$	3
$T_2 \leq t_{TCA}$	$P_{C_b} \geq P_{C_0}$	-	2
	$P_{C_b} < P_{C_0}$	$Pl - Bel \leq \Delta$	4
		$Pl - Bel > \Delta$	3

if the evidence does not support the fact that it poses neither high risk nor low risk, it is so close in time to the encounter that an action should be done. Class 2 indicates a CAM should be considered, although it is possible to collect better data that reduces the uncertainty. On the other side, Class 4 includes cases that posse a low risk, but far enough in time to the encounter it is still possible to collect better information before making a final decision, while Class 5 indicates that the event is close in time but poses no actual risk. Finally, Class 3 includes those cases where the encounter is not immediate but the evidence does not support either high or low risk, and more information needed would be needed.

In Fig. 4, there is an example of the class distribution of a set of 9000 encounter geometries according to the evidence-based criterion. The thresholds used for the criterion are detailed in Table 3. Blue and black colours are associated with cases with high $\hat{P}_C$ when using only with Eq. (2), while red and pink colours with cases with low $\hat{P}_C$ when computed with that equation

Table 3: Classification thresholds for the evidence-based criterion

Parameter	**Value**
Probability of Collision (P_{C_0})	4.4 x 10^{-4}
Degree of confidence (Δ)	0.3
Belief (Bel_0)	0.5
Lower time threshold (T_1)	2 days
Upper time threshold (T_2)	4 days

The samples have been obtained from 5 different encounter geometries, differentiated in whether both

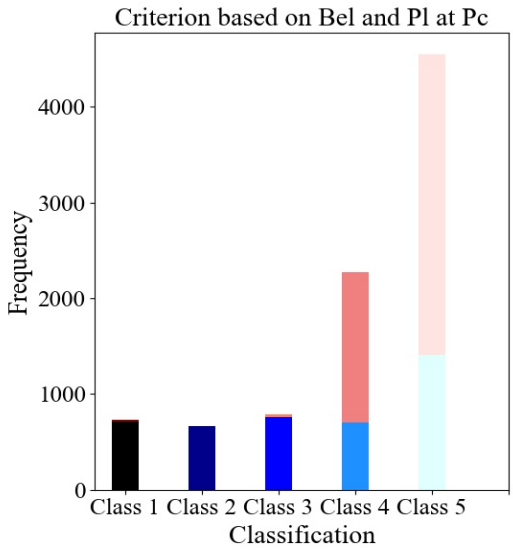

Fig. 4: Histogram showing the distribution among classes according to the evidence-based classification criterion. Blue/black colours represent samples classified as "Collision" by a purely probabilistic approach, red/pink colours shows samples classified as "No Collision" by a probabilistic approach.

sources give coherent or contradictory information and whether the proposed set of ellipses are close or far from the HBR: i) Geo. 1, ellipses overlapping and both overlapping HBR, ii) Geo. 2, ellipses overlapping and none overlapping HBR, iii) Geo 3. ellipses not overlapping and only one overlapping HBR, iv) Geo. 4, ellipses not overlapping and none overlapping HBR, v) Geo. 5, ellipses not overlapping and both overlapping HBR. The samples have been associated with different times to the TCA so that they represent immediate ($t < T_1$), mid-term ($T_1 < t < T_2$) or long term ($t > T_2$) encounters. Three different *bpa* assignment to the sources have been made: equally reliable ($bpa_1 = bpa_2 = 0.5$), Source 1 more reliable ($bpa_1 = 0.9, bpa_2 = 0.1$) and Source 2 more reliable ($bpa_1 = 0.1, bpa_2 = 0.9$). More details can be found in Sanchez and Vasile.[4]

3.2 *Intelligent Classification System*

The performances of an Intelligent Classification System based on the previous evidence-based classification criterion are presented in this section.

This Intelligent Classification System (ICS) was first presented in Sanchez and Vasile.[4] More details on the databases used for training, the ML techniques comparison analysis and the best model hyper-parameters can be found in there.

Table 4: Intelligent Classification System performances.

	Accuracy	**Training time [s]**	**Validation time [s]**
Overall	93.3	7.5443	0.555
		Recall	**Precision**
Class 1		98.7	88.4
Class 2		97.4	83.5
Class 3		77.7	82.9
Class 4		92.4	99.2
Class 5		92.4	99.2

The ICS takes as inputs the time to the TCA, the interval bounds of the uncertain variables on the B plane ($[\mu_\xi, \mu_\zeta]$, $[\sigma_\xi, \sigma_\zeta]$) for each source of information and the *bpa* associated with the sources, which makes a total of 19 inputs, in the case two sources of information are considered. As output, the system provides the class according to the evidence-based classification criterion and thus, the suggested action to be taken by the STM operators. The system uses Random Forest (RF)[8] as the surrogate ML-based model since it presented the highest level of accuracy and the shortest training time among the techniques studied in Sanchez and Vasile.[4]

The main advantage of this intelligent system is that it allows to autonomously predict the risk associated with an event and suggest the best action given an uncertain close encounter geometry. In addition to that, it takes into account epistemic uncertainty and speeds up the process since it allows to skip the explicit computation of Pl and Bel, which can be time-consuming if several sources of information are considered.

Table 4 presents the performances of the Intelligence Classification System over the 5,760 samples on the "Validation Set", having been trained with the "Training Set", both detailed in Sanchez and Vasile.[4] The accuracy (the percentage of samples correctly predicted over all the samples) has been calculated over all the samples in the database, while the precision (the percentage of the samples correctly predicted from a certain class over the total number of samples predicted on this class) and recall (the percentage of samples correctly predicted on a certain class over the total number of samples in that class) have been computed by classes. The training and validation times over the whole sets can be also found

in Table 4.

4. COLLISION AVOIDANCE MANOEUVRE

According to the evidence-based classification criterion, the risk associated with an event can give as an output of the Intelligent Classification System that a CAM is required. Understood under the perspective of a global Intelligent Agent that support STM operators in all the Collision Risk Assessment process, the output of the ICS can lead to a blank space where the Collision Avoidance Manoeuvre should be computed (Fig. 5).

In this section, the computation of the optimal CAM under epistemic uncertainty in order to fill that space is presented.

4.1 *CAM Linear Model*

This section introduces the Linear Model for computing an optimal impulse given its magnitude for avoiding a space close encounter.

Following Vasile and Colombo,[9] the instantaneous variation of orbital elements $\delta\mathbf{x} = [\delta a, \delta e, \delta i, \delta\Omega, \delta\omega, \delta M_{t_m}]^T$ due to a variation of velocity vector $\delta\mathbf{v} = [\delta v_t, \delta v_n, \delta v_h]^T$ along the tangential, normal and out-of plane directions, $<T, N, H>$, can be computed with the linear transformation:

$$\delta\mathbf{x} = \mathbf{G}\delta\mathbf{v} \quad [13]$$

where the matrix $\mathbf{G}$ is defined in Eq. (14).

The subscript "$_m$" refers to the manoeuvre position, b is the semi-minor axis $b = a\sqrt{1-e^2}$, p the semi-latus rectum $p = b^2/a$, h the specific angular momentum $h = nab$, n is the mean motion $n = \sqrt{\mu/a^3}$, and r_m and v_m are the unperturbed position and velocity of the satellite at manoeuvre. The variation in position of the satellite (expressed in the $<R, T, H>$) at encounter time t_c, or Time of Closest Approach (TCA), after deviation with respect to the unperturbed orbit can be approximated with the linear model:[9]

$$\delta\mathbf{r} = \mathbf{A_t}\delta\mathbf{x} \quad [15]$$

where the matrix $\mathbf{A_t}$ is defined in Eq. (16), being $\Delta t = t_c - t_m$ the elapsed time between the manoeuvre and the TCA. The subscript "$_c$" refers to the encounter position. Note that the variation in mean anomaly, M, is made of two terms:

$$\delta M = \delta M_{t_m} + \delta M_n \quad [17]$$

where the first term comes from the change on mean anomaly due to the manoeuvre and it is included on $\mathbf{G}$:

$$\delta M_{t_m} = -\frac{b}{eav_m}\left[2\left(1+\frac{e^2 r_m}{p}\right)\sin\theta_m \delta v_t + \right. \\ \left. + \frac{r_m}{a}\cos\theta_m \delta v_n\right] \quad [18]$$

and the second term refers to the delay at TCA due to the change in the semi-major axis:

$$\delta n = \sqrt{\frac{\mu}{a^3}} - \sqrt{\frac{\mu}{(a+\delta a)^3}} \quad [19]$$

This second term, δM_n, is included in $\mathbf{A_t}$ after approximate it as:

$$\delta M_n = \delta n \Delta t = -\frac{3}{2}\frac{\sqrt{\mu}}{a^{\frac{5}{2}}}\Delta t \delta a \quad [20]$$

Being $\mathbf{G}$ the matrix mapping the $\delta\mathbf{v}$ to the variation of the parameters and $\mathbf{A_t}$ the matrix mapping the variation of the parameters into the variation of the position vector, $\delta\mathbf{r}$, from this deflection the impact parameter B at the encounter time can be computed. The deflection vector $\delta\mathbf{x}_b$ in the B-plane coordinates can be expressed as:

$$\delta\mathbf{x}_b = [\delta\xi \;\; \delta\eta \;\; \delta\zeta]^T = \left[\hat{\xi} \;\; \hat{\eta} \;\; \hat{\zeta}\right]^T \delta\mathbf{r} = \mathbf{B}\delta\mathbf{r} \quad [21]$$

where:

$$\hat{\eta} = \frac{\mathbf{U}_d}{U_d}, \quad \hat{\xi} = \frac{\mathbf{v}_{sc} \wedge \hat{\eta}}{\|\mathbf{v}_{sc} \wedge \hat{\eta}\|}, \quad \hat{\zeta} = \hat{\xi} \wedge \hat{\eta} \quad [22]$$

and $\mathbf{U_d}$ is the relative velocity at impact time ($\mathbf{v_1} - \mathbf{v_2}$) and $\mathbf{v_{sc}} = \mathbf{v_1}$ is the velocity of the incoming satellite at encounter time, both expressed in the same reference frame. The impact parameter B is then defined as:

$$B = \sqrt{\xi^2 + \zeta^2} = \sqrt{(\xi_0 + \delta\xi)^2 + (\zeta_0 + \delta\zeta)^2} \quad [23]$$

and provides an estimation of the miss-distance.

Calling $\mathbf{B}$ the matrix mapping the variation of the position vector to the B-plane. Then for a pure Keplerian motion we have:

$$\delta\mathbf{x_b} = \mathbf{B}\mathbf{A_t}\mathbf{G}\delta\mathbf{v} \quad [24]$$

and in compact form:

$$\delta\mathbf{x_b} = \mathbf{T}\delta\mathbf{v} \quad [25]$$

Considering the centre of the uncertain ellipse projected on the B-plane before the impulse is given by $\mathbf{r_e} = [\xi_0, 0, \zeta_0]^T$. A CAM can be implemented so that the distance to the centre of the ellipse is maximised

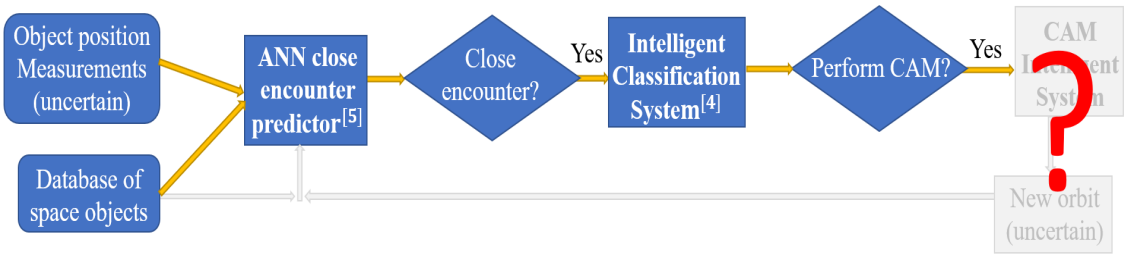

Fig. 5: Intelligent Agent to support STM with no block computing the optimal CAM.

$$\mathbf{G} = \begin{bmatrix} \frac{2a^2 v_m}{\mu} & 0 & 0 \\ \frac{2(e+\cos\theta_m)}{v_m} & -\frac{r_m}{a v_m}\sin\theta_m & 0 \\ 0 & 0 & \frac{r_m\cos(\omega+\theta_m)}{h} \\ 0 & 0 & \frac{r_m \sin(\omega+\theta_m)}{h\sin i} \\ \frac{2\sin\theta_m}{e v_m} & \frac{2e+(r_m/a)\cos\theta_m}{e v_m} & -\frac{r_m\sin(\omega+\theta_m)\cos i}{h\sin i} \\ -2\frac{b}{e a v_m}\left(1+\frac{e^2 r_m}{p}\right)\sin\theta_m & -\frac{b}{e a v_m}\frac{r_m}{a}\cos\theta_m & 0 \end{bmatrix} \quad [14]$$

$$\mathbf{A_t}^T = \begin{bmatrix} \frac{r_c}{a} - \frac{3}{2}\frac{e\sin\theta_c}{\mathbf{1-e^2}}\frac{\sqrt{\mu}}{a^{\frac{3}{2}}}\Delta t & -\frac{3}{2}\frac{r_c}{(\sqrt{1-e^2})^3}(1+e\cos\theta_c)^2\frac{\sqrt{\mu}}{a^{\frac{5}{2}}}\Delta t & 0 \\ -a\cos\theta_c & \frac{r_c\sin\theta_c}{1-e^2}(2+e\cos\theta_c) & 0 \\ 0 & 0 & r_c\sin(\omega+\theta_c) \\ 0 & r_c\cos i & -r_c\cos(\omega+\theta_c)\sin i \\ 0 & r_c & 0 \\ \frac{ae\sin\theta_c}{\sqrt{1-e^2}} & \frac{r_c}{(\sqrt{1-e^2})^3}(1+e\cos\theta_m)^2 & 0 \end{bmatrix} \quad [16]$$

(*max B parameter* problem) or so that the Probability of Collision is minimised (*min* P_C problem). The assumption is that in the limit of the linear model the ellipsoid of uncertainty translates rigidly without deforming or rotating. This is not true in general and represents an approximation introduced by our method. In the following, the magnitude of the impulse, δv_0, is assumed to be known and constant only optimising the direction of the manoeuvre and only the optimisation of the P_C will be explained.

4.1.1 *Minimisation of the Probability of Collision*

In this problem the CAM is selected so that the Probability of Collision, P_C, of the event is minimised. The short-encounter assumptions hold[15] and Eq. (1) is used to compute the P_C.

According to that equation, for minimising P_C one needs to maximise the exponent inside the integral. Let us consider the uncertainty ellipse on the B-plane with covariance:

$$\mathbf{\Sigma} = \begin{bmatrix} \sigma_\xi^2 & \sigma_{\xi\zeta} \\ \sigma_{\xi\zeta} & \sigma_\zeta^2 \end{bmatrix} \quad [26]$$

with determinant $\Delta = \sigma_\xi^2\sigma_\zeta^2 - \sigma_{\xi\zeta}^2$ and inverse:

$$\mathbf{\Sigma}^{-1} = \frac{1}{\Delta}\begin{bmatrix} \sigma_\zeta^2 & -\sigma_{\xi\zeta} \\ -\sigma_{\xi\zeta} & \sigma_\xi^2 \end{bmatrix} \quad [27]$$

Thus assuming that the centre of the coordinates is in the centre of the ellipse then we want to maximise the following quadratic form under the assumption that the manoeuvre will rigidly translate the ellipse:

$$\begin{aligned} &\max_{\delta\mathbf{v}}\left(\delta\mathbf{v}^T\mathbf{T}^T\mathbf{\Sigma^{-1}}\mathbf{T}\delta\mathbf{v}\right) \\ &s.t. \\ &\mathbf{r_e}\cdot\mathbf{T}\delta\mathbf{v} > 0 \end{aligned} \quad [28]$$

Thus, the minimisation problem can be solved by finding the vector, $\delta\mathbf{v_{opt}}$, parallel to the eigenvector $\mathbf{s_1}$ conjugated to the maximum eigenvalue of the matrix $\mathbf{T}^T\mathbf{\Sigma}^{-1}\mathbf{T}$ with magnitude δv_0:

$$\delta\mathbf{v_{opt}} = \delta v_0\mathbf{s_1} \quad [29]$$

4.2 *Optimal manoeuvre under epistemic uncertainty*

As indicated in Section 2, the uncertainty on the satellite position has an epistemic component, which affects the computation of the optimal CAM.

Under the assumptions of the Dempster-Shafer Theory of Evidence (DSt) introduced above, it is possible to account for the epistemic uncertainty when computing the optimal CAM. Assuming the encounter geometry is known and affected by uncertainty, the same approach used for the risk assessment can be followed here. In the remainder of the paper the uncertain variables are assumed to be given by the sources of information in the form of intervals including the true value but with no further assumptions on the distribution within the interval. The uncertain space can be the same as for the classification criterion, although it can be easily extended to a more generic case. Thus, the uncertain vector considered in the following will be composed by the miss distance, $[\mu_x i, \mu_z eta]$, and the covariance terms on the B plane, $[\sigma_\xi^2, \sigma_\zeta^2, \sigma_{\xi\zeta}]$.

The uncertainty in the position of an object is translated in an uncertainty in the orbital parameters at the time of execution of the CAM and then propagated and projected onto the B plane using matrix $\mathbf{BA_t}$, obtaining the corresponding bound limits of the set of uncertain variables on the B plane. A set of values for the uncertain variables corresponds to families of uncertainty ellipses on the B plane.

This implies that one has to minimise the P_C that corresponds to the worst ellipse. Thus one needs to solve a min-max problem to find the optimal impulse that minimises the Probability of Collision for the worst-case scenario within each Focal Element (FE). The worst-case scenario is the value of the uncertain variables within the bound of the FE that yields the highest Probability of Collision. The algorithm presented in Vasile,[13] extended by Filippi,[14] is used for solving the following min-max optimisation problem:

$$\begin{aligned} &\min_{\delta\mathbf{v}} \max_{\mathbf{u}\in\Omega_u} P_C \\ &s.t. \\ &\mathbf{r_e}\cdot\delta\mathbf{v} > 0 \end{aligned} \qquad [30]$$

where P_C is computed using Eq. (1).

As shown previously, the minimisation of P_C is equivalent to find the eigenvector associated with the maximum eigenvalue of the matrix $\mathbf{T}^T\mathbf{\Sigma}^{-1}\mathbf{T}$ in Eq. (28). Thus, the minimisation step in the min-max algorithm has been performed analytically. During the iteration (see Algorithm in Vasile[13] for more details), the matrix $\mathbf{T}^T\mathbf{\Sigma}^{-1}\mathbf{T}$ has been replaced by $\mathbf{T^T A T}$, where $\mathbf{A}$ is the sum of the inverse covariance matrices of the worst-case ellipses found so far: $\mathbf{A} = \mathbf{\Sigma_1^{-1}} + \mathbf{\Sigma_2^{-1}} + ...$

The maximisation step to find the worst-case ellipse given the $\delta\mathbf{v_{opt}}$ from the minimisation step has been carried out using a numerical optimiser applied directly to the function (1). Given the nature of the linear model and the fact that the manoeuvre does not change the shape of the uncertainty region on the B-plane but simply translates it in the same plane, the convergence is quite fast and require only a handful of iterations.

4.3 *Propagation of the uncertainty*

Assuming that the initial mean and covariance are given in orbital elements at a time t_0. Then we can use the matrices $\mathbf{B}$ and $\mathbf{A_t}$ to propagate them to the TCA. A pure Keplerian motion is considered.

4.3.1 *Propagation of the mean*

The mean value can be propagated using the matrix $\mathbf{B}$ and $\mathbf{A_t}$ assuming close motion respect to a nominal value. A nominal value is considered a reference orbit used for detecting close approaches. In a pure aleatory uncertainty scenario, mean and nominal value coincide. If accounting for epistemic uncertainty being quantified in the form of intervals, the mean value of each uncertain ellipsoid will be different, in general, than the nominal value.

Thus, if we have the mean orbital elements at time t_0 expressed as intervals we need to compute (for each value in a FE) the corresponding mean value on the B plane by using the $\mathbf{BA_t}$ matrix. Since the differences in Keplerian element are not due to a change on velocity but due to the uncertainty itself, the matrix $\mathbf{G}$ is not needed for uncertainty propagation. Let's call $\boldsymbol{\mu_e}(t_0) \in \gamma_\mu$ the mean value of the orbital elements at time t_0 and γ_μ the corresponding FE, then from the matrix $\mathbf{BA_t}$ one gets the variation of position on B plane coordinates:

$$\delta\mathbf{r}_{\mathbf{e}_\mu} = \mathbf{BA_t}\left(\boldsymbol{\mu_e}(t_0) - \mathbf{q}(t_0)\right) \qquad [31]$$

where $\mathbf{q}(t_0)$ are the nominal Keplerian elements at initial time.

The miss distance in B plane associated with the mean can be obtained by:

$$\mathbf{r}_{\mathbf{e}_\mu} = \mathbf{r_e} + \delta\mathbf{r}_{\mathbf{e}_\mu} \qquad [32]$$

4.3.2 *Propagation of the covariance matrix*

From $\mathbf{D}(t_0)$, the covariance of the orbital parameters at time t_0 and assumed diagonal, one has to compute the covariance $\mathbf{\Sigma}$ of the relative position on the B plane that defines the projected uncertain ellipse.

Again, if the covariance is only diagonal and each component $\sigma_e \in \gamma_\sigma$ belongs to a FE, for each value

Table 5: Nominal orbital elements at time 4438.2 s before the TCA.

	Nominal 1	**Nominal 2**
SMA (a)	7006.79	6295.53
ecc. (e)	$5.5{\cdot}10^{-4}$	$6.684{\cdot}10^{-1}$
inc. (i)	1.332	2.029
RAAN (Ω)	0.154	6.121
Arg. Per. (ω)	$5.710{\cdot}10^{-2}$	3.408
True Anom. (θ)	5.810	2.422

Table 6: Uncertain orbital parameters interval bounds.

	Mean	$\mathbf{D_0}$**diagonal**
a	7006.3 7007.5	$4.5132{\cdot}10^{-4}$ $5.962{\cdot}10^{-2}$
e	$5.499{\cdot}10^{-4}$ $5.501{\cdot}10^{-4}$	$5.298{\cdot}10^{-10}$ $5.907{\cdot}10^{-8}$
i	1.331 1.332	0.0 0.0
Ω	0.153 0.154	$3.273{\cdot}10^{-8}$ $5.644{\cdot}10^{-7}$
ω	$5.709{\cdot}10^{-2}$ $5.710{\cdot}10^{-2}$	$4.511{\cdot}10^{-8}$ $3.326{\cdot}10^{-7}$
θ	5.809 5.810	$4.802{\cdot}10^{-8}$ $4.746{\cdot}10^{-7}$

within the FE we have a value of the components of $\mathbf{D}(t_0)$. For each of those values, we then need to use again the transformation $\mathbf{BA_t}$ to compute the corresponding values on the B-plane. Similarly to the propagation of the mean, one can compute the variation on the B plane for each value with respect to the mean within each FE:

$$\delta\mathbf{r}_{\mathbf{e}_\sigma} = \mathbf{BA_t}\left(\boldsymbol{\sigma_e}(t_0) - \boldsymbol{\mu_e}(t_0)\right) \quad [33]$$

The actual miss distance on the B plane can be computed as:

$$\mathbf{r}_{\mathbf{e}_\sigma} = \mathbf{r}_{\mathbf{e}_\mu} + \delta\mathbf{r}_{\mathbf{e}_\sigma} \quad [34]$$

4.4 *Validation of Linear Model*

On the following, a numerical example to illustrate the CAM min-max optimisation using the Linear Model is presented. Table 5 includes the initial nominal orbital parameters of the two satellites at the initial time $t_0 = 4438.2$ s before the TCA. The initial orbital parameters are affected by both, aleatory and epistemic uncertainty (Table 6). The aleatory uncertainty is modelled by a 6D-Normal Distribution with a diagonal covariance matrix $\mathbf{D_0}$. The epistemic uncertainty is quantified by intervals of the mean and covariance of the initial orbital elements. The matrix $\mathbf{BA_t}$ has been used to propagate the uncertainty to the B plane and 20 ellipsoids have been withdrawn for the initial set of ellipsoids to obtain the interval bounds of the uncertain variables at the B plane. The optimal CAM has been computed for three orbits before the TCA at 4 points per orbit, measured as angular position in the true anomaly, $\Delta\theta$. The magnitude of the impulse is assumed to be constant and equal to $\delta v_0 = 10$ cm/s. Only one source of information is considered, and thus, only one FE.

Fig. 6a includes some of the uncertain ellipses projected on the B plane. It illustrates the situation before computing the CAM. Since there is not only one, but a set of them, it is necessary to find the impulse that optimises the worst-case ellipse at each manoeuvre position. Fig. 6b includes the worst-case scenario parameters (dash blue) as a function of $\Delta\theta$ and the FE bounds (solid green and yellow). It can be seen that some parameters are almost constant while others change with $\Delta\theta$, indicating a change on the worst-case ellipse depending on the execution instant of the manoeuvre. In Fig. 6c, the unitary vector parallel to the optimal impulse that minimises the worst-case scenario at each $\Delta\theta$ is included (top: $\hat{\delta v_t}$, middle: $\hat{\delta v_n}$, bottom: $\hat{\delta v_h}$). Finally, Fig. 6d shows the P_C evolution as a function of the $\Delta\theta$ at which the manoeuvre is applied. The solid lines represent the P_C associated with the ellipses in Fig. 6a, while the dashed line indicated the P_C evolution of the worst-case scenario. As expected, the worst-case scenario poses a higher risk at any $\Delta\theta$.

4.5 *ML for CAM*

After obtaining the results of the min-max optimisation of the optimal impulse and having in mind the Intelligent Classification System, the path for the design of a ML-based system able to predict the optimal CAM accounting for epistemic uncertainty is indicated in this last section.

Such a system should predict the three components of the optimal impulse for the worst-case scenario given the uncertain state and the time to the TCA. Thus, it will have the same inputs of the Intelligent Classification System: the interval bounds of the uncertain variables of the encounter geometry and the bpa of the source (11 inputs per source) plus the time to the TCA, or any other analogue measurement, like the angular distance to the encounter in True Anomaly, $\Delta\theta$ or in Mean Anomaly, ΔM.

With this system along with those ML-based models proposed in previous works by the authors,[4,5] it could be possible to build an Intelligent Agent able to completely support the STM operators from the detection of close encounter when uncertain position measurements are received, to the risky classification

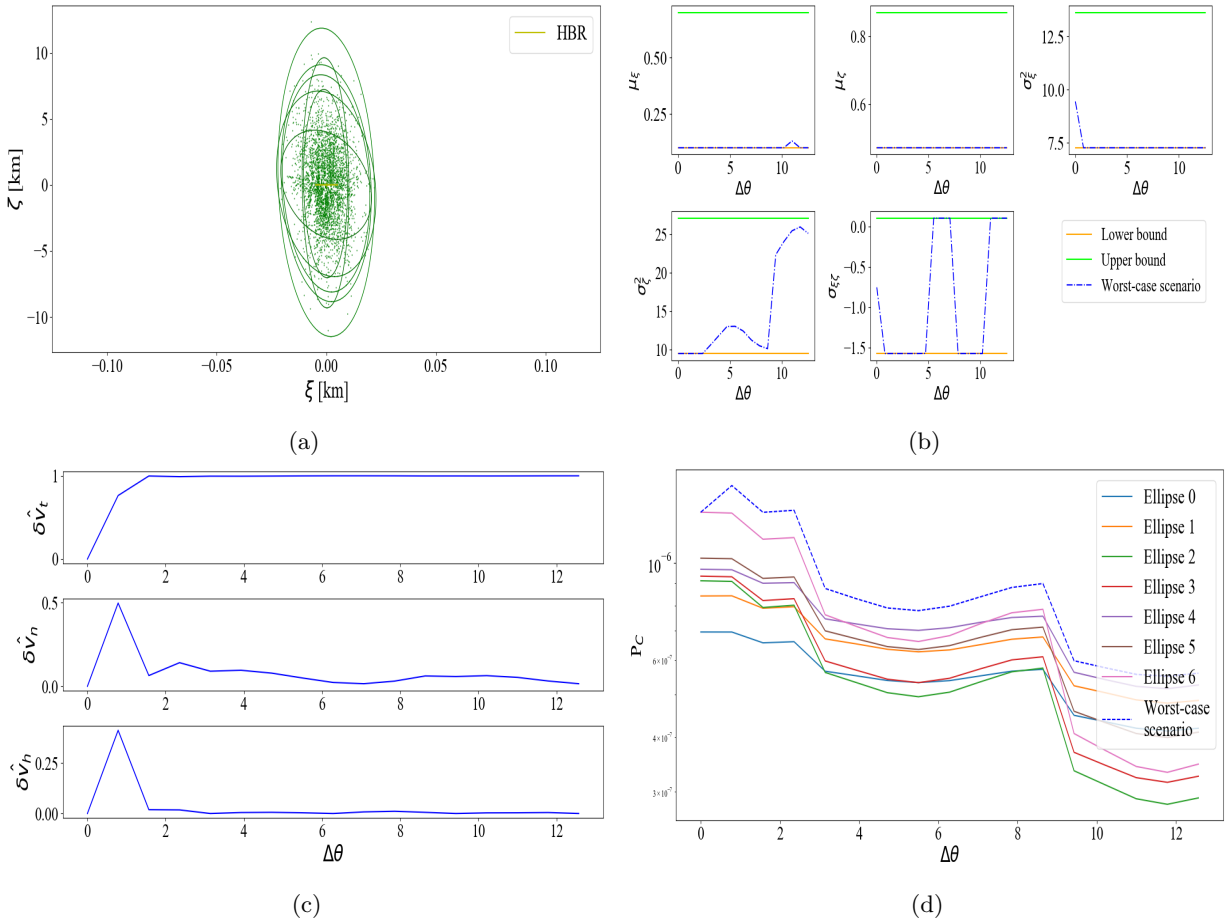

Fig. 6: Min-max CAM optimisation using Linear Model. (a) Uncertain ellipses on B plane affected by epistemic uncertainty. (b) Worst-case scenario uncertain variables (dash blue) and FE interval bounds (solid green and yellow). Top-left: μ_ξ, top-centre: μ_ζ, top-right: σ^2_ξ, bottom-left: σ^2_ζ, bottom-centre: $\sigma_{\xi\zeta}$. (c) Optimum impulse unitary parallel vector, $\hat{\delta\mathbf{v}}$: Top: $\hat{\delta v}_t$, middle: $\hat{\delta v}_n$, bottom: $\hat{\delta v}_h$. (d) P_C evolution after applying the optimal impulse: (solid lines) ellipses in Fig. 6a, (dash line) worst-case scenario ellipse.

of them, the computation of the optimal CAM when they pose high risk and the closure of the loop recomputing potential close encounters along the new modified orbit (Fig. 7). The development of this last block of the Intelligent Agent will be presented in future works.

5. CONCLUSIONS

In this paper, we introduced a simple calculation of an optimal CAM to be included in an Intelligent Classification System (ICS) that automatically predicts the collision risky and suggest CAM executions. This system, based on Random Forests, presents high accuracy (above 90%) and very low run times (below 1 s).

Both the ICS and the CAM calculation method accounts for epistemic uncertainty in the calculation of the probability of collision and manoeuvre execution. This uncertainty has been quantified, under the Dempster-Shafer Theory of Evidence, in the form of intervals with associated basic probability mass but with no assumptions on the probability distribution within each interval.

The CAM computation method solves a min-max problem to find the optimal manoeuvre for the worst-case uncertain ellipse.

In further works, we will present a ML-based CAM definition system in order to close the loop between collision prediction and CAM execution.

References

[1] G. Peterson, M. Sorge, and W. Ailor. Space traffic management in the age of new space. *Center for Space Policy and Strategy. The Aerospace Corporation*, 4 2018.

[2] H. Lewis, J. Radtke, A. Rossi, J. Beck, M. Oswald, P. Anderson, B. Bastida Virgili, and H. Krag. Sensitivity of the space debris environment to large constellations and small satellites. *Journal of the British Interplanetary Society*, pages 105–117, 2017.

[3] T. Muelhaupt, M. Sorge, J. Morin, and R. Wilson. Space traffic management in the new space era. *The Journal of Space Safety Engineering*, 6:80–87, 6 2019.

[4] L. Sánchez and M. Vasile. On the Use of Machine Learning and Evidence Theory to Improve Collision Risk Management. *Acta Astronautica. ICSSA-2020 Special Issue*, In Press, 2020.

[5] L. Sánchez, M. Vasile, and E. Minisci. AI to Support Decision Making in Collision Risk Assessment. *70th International Astronautical Congress. Washington DC, USA*, Oct 2019.

[6] H. Peng and X. Bai. Exploring capability of support vector machine for improving satellite orbit prediction accuracy. *Journal of Aerospace Information Systems*, 15(6):366–381, 2018.

[7] R. Abay, M. Brown, R. Boyce, and A. Karacor. Open Source Collision Avoidance Maneuver Planning Tool. *68th International Astronautical Congress (IAC), Adelaide, Australia*, 09 2017.

[8] L. Breiman. Random forest. *Machine Learning*, 45:5–32, 10 2001.

[9] M. Vasile and C. Colombo. Optimal Impact Strategies for Asteroid Deflection. *Journal of Guidance, Control and Dynamics*, 31(4):858–872, Jul-Aug 2008.

[10] R Abay. Collision Avoidance Dynamics for Optimal Impulsive Collision Avoidance Maneuvers. *8th International Conference on Recent Advances in Space Technologies, Istanbul, Turkey*, 06 2017.

[11] C. Bombardelli and J. Hernando-Ayuso. Optimal Impulsive Collision Avoidance in Low Earth Orbit. *Journal of Guidance, Control and Dynamics*, 38(2):217–225, Feb 2015.

[12] G. Shafer. *A Mathematical Theory of Evidence*. Princeton University Press, 1976, Princeton, NJ, 1 edition, 4 1976.

[13] M. Vasile. On the Solution of Min-Max Problems in Robust Optimization. *The EVOLVE of Guidance, Control and Dynamics International Conference, Beijing, China*, Jul 2014.

[14] G. Filippi and M. Vasile. A Memetic Approach to the Solution of Constrained Min-Max Problems. *IEEE CEC 2019, Wellington, New Zealand*, 06 2019.

[15] R Serra, D. Arzelier, M. Joldes, J.B. Lasserre, A. Rondepierre, and B. Salvy. Fast and Accurate Computation of Orbital Collision Probability for Short-Term Encounters. *Journal of Guidance, Control, and Dynamics*, 39:1–13, 01 2016.

[16] S. Alfano and D. Oltrogge. Probability of collision: Valuation, variability, visualization, and validity. *Acta Astronautica*, 148:201–316, 4 2018.

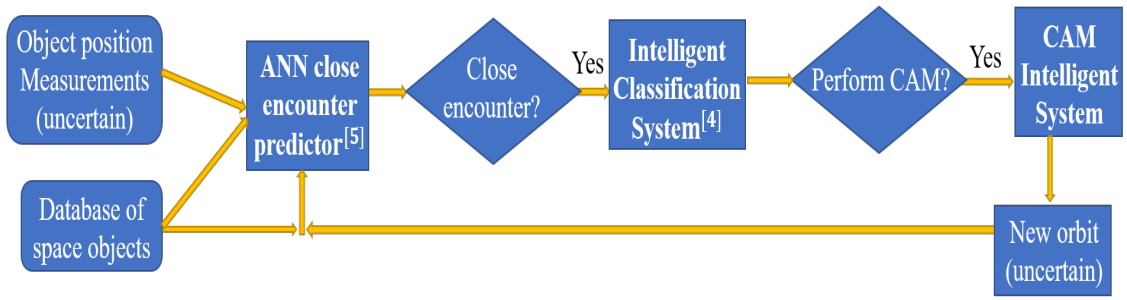

Fig. 7: Intelligent Agent to support STM operators with the block to automatically compute the optimal CAM.

[17] M. Balch, R. Martin, and S. Ferson. Satellite Conjunction Analysis and the False Confidence Theorem. *Proceedings of the Royal Society A: Mathematical, Physical and Engineering Sciences*, 475, 7 2019.

[18] L. Newman, M. Hejduk, R. Frigm, and M. Duncan. Evolution and implementation of the nasa robotic conjunction assessment risk analysis concept of operations. *Advanced Maui Optical and Space Surveillance Technologies Conference, Maui, Hawaii, USA*, 9 2014.

[19] K. Merz, B. Bastida Virgili, V. Braun, T. Hlohrer, Q. Funke, H. Krag, S. Lemmens, and J. Siminski. Current collision avoidance service by esa's space debris office. *Proc. 7th European Conference on Space Debris, Darmstadt, Germany*, 4 2017.